



Energy Conversion and Management: X

Volume 20, October 2023, 100440

Optimization and thermo-economic performance of a solar-powered vapor absorption cooling system integrated with sensible thermal energy storage


Dinesh Kumar Sharma ^{a b}  , Dilip Sharma ^b, Ahmed Hamza H. Ali ^c

^a Department of Mechanical Engineering, Swami Keshvanand Institute of Technology, Management and Gramothan, Jaipur 302017, India

^b Department of Mechanical Engineering, Malaviya National Institute of Technology, Jaipur 302017, India

^c Department of Mechanical Power Engineering, Faculty of Engineering, Assiut University, Assiut 71516, Egypt

Received 26 May 2023, Revised 13 August 2023, Accepted 14 August 2023, Available online 21 August 2023, Version of Record 25 August 2023.

 [What do these dates mean?](#)



Show less 

 Outline |  Share  Cite

<https://doi.org/10.1016/j.ecmx.2023.100440> 

[Get rights and content](#) 

Under a Creative Commons [license](#) 

open access

Abstract

Higher demand for refrigeration systems adversely affects power grids, causing blackouts, increased electricity expenses, and carbon emissions. However, using renewable energy thermally driven refrigeration absorption systems is a promising alternative. The higher initial cost and dependency on local weather, large space area for installation, and complex design are hurdles for the widespread of these systems compared to the conventional vapor compression refrigeration systems. This study uses response surface methodology to model a real vapor absorption machine (VAM) incorporated

with the measured data. This VAM is the refrigeration machine of a solar-powered absorption cooling system (SPACS) integrated with thermal energy storage for milk chilling installed and operated in Jaipur (India). The weather data for 2022 is used in performance and productivity analysis in this study. The results show that most of the summer months, the system can produce desired cooling to take down the 1000l of milk within 3h as per standards ISO 5708 – 2 II. Moreover, the solar loop still has sufficient driving heat to charge the 1000l cold storage tank/another milk tank. During winter days, it takes a significant system response time (SRT) to reach the thermal energy storage (TES) up to 95°C; after that, VAM operates significantly underperforming due to weak solar insolation; even the system cannot provide cooling to the first milking. The system produces monthly cooling energy of up to 2356 kWh in summer and is reduced to 620 kWh during monsoon and winter. The maximum value of the coefficient of performance (COP_{VAM}) is achieved as 0.55 with an average of 0.41–0.46 during summer months whereas 0.34–0.39 during monsoon and winter days. The system's energy efficiency ratio (EER) ranges from 2.5 to 6.5, with an overall average of 4.55, which is far better than the conventional vapor compression refrigeration systems. The LCOE for the SPACS has been estimated to be 0.177 \$/kWh, whereas the simple payback period is 12.4years, and the discounted payback period is 19.7years.

[<](#) PreviousNext [>](#)

Keywords

Solar absorption cooling; Thermal energy storage; Response surface methodology; Energy efficiency; Milk chilling

Nomenclature

CC

construction/installation cost

CF

cash inflows

DPBP

discounted payback period

ET-CPC

evacuated tube with compound parabolic concentrator

LCOE

levelized cost of energy

RTD

resistance temperature detector

SPACS

solar-powered absorption cooling system

SPBP

simple payback period

SRT

system response time

TES

thermal energy storage

TLCC

total life cycle cost

VAM

vapor absorption machine

Symbols and notations

A

area (m²)

b

thickness (m)

C_p

specific heat (J/kg.K)

COP_{VAM}

coefficient of performance

D

tube diameter (m)

EER

energy efficiency ratio

f

friction factor

F_R

heat removal factor

I_T

solar insolation (W/m²)

L

length (m)

m_f

mass flow rate (kg/s)

P

pressure (kPa)

Q_{useful}

useful heat gain (kW)

 Q_{Cooling}

cooling capacity (kW)

 V

fluid velocity (m/s)

 U_L overall heat coefficient ($\text{W}/\text{m}^2\cdot\text{K}$)

Greek letter

 α absorptivity ρ

density

 η

efficiency

 μ kinematic viscosity k thermal conductivity τ transmissivity

Subscript

amb

ambient

c

collector

CHW

chilled water

CW

cooling water

f

fluid

HW

hot water

in

inlet

m

mean

N

number of years

n

number of collector in-series

out

outlet

r

discount rate

1. Introduction

Higher demand for refrigeration systems adversely affects power grids, causing blackouts, increased electricity expenses, and carbon emissions. However, using renewable energy-driven refrigeration absorption systems (SPACS) is a promising alternative [1]. The higher initial cost and dependency on local weather, large space area for installation, and complex design are hurdles for the widespread of these systems compared to the conventional vapor compression refrigeration systems [2]. It is reported from the previous studies that optimizing the solar collectors, incorporating thermal energy storage (TES), regular maintenance, and integration with appropriate applications can all help to enhance the productivity and performance of solar absorption cooling systems [3], [4].

In recent times, substantial progress has been achieved in the technological evolution of SPACS. Consequently, research emphasis has pivoted towards tackling the system-level complexities associated with the proficient design and effective operational control of fully integrated setups. The study on feasibility and viability needs to be done case by case as per the environmental conditions in which the system is to be installed [5]. Along with this, the scale of operation also plays a decisive role while examining the viability of SAPCS. It is reported that conventional vapor compression systems are more likely to be adopted at residential scales (5–15 kW) than solar thermal cooling systems, as the latter has a significantly higher first cost [6]. However, for large-scale applications (>50 kW), the economies of scale can make larger solar thermal cooling units economically more feasible [7].

The estimation of productivity and performance of SPACS are subjected to appropriate modelling of its components and optimized thermal management practices. It has been noted that most of the studies are based on the thermodynamic modelling of the absorption system [8], [9]. Khan et al. [10] modeled the single-effect vapor absorption cooling system with TRNSYS. The thermodynamic modeling of SPACS is based on the principles of thermodynamics, which are well-established and have been extensively studied. The models consider the heat transfer mechanisms, mass transfer, and thermodynamic properties of the working fluids. However, simplified assumptions, uncertainty of data, and complex interactions are some of the reasons for the increasing gap between the actual and estimated productivity and performance of SPACS. Solar absorption cooling systems are complex

systems that involve various interactions between components, such as solar collectors, absorption chillers, cooling towers, TES, and heat exchangers. These interactions can be challenging to model accurately.

Furthermore, environmental conditions are dynamic, whereas most research uses nondynamic operating conditions. Hence, there is a need to investigate the systems' performance and optimize the SPACS for the subsystems sizing and their interactions using dynamic modelling. Many researchers [11], [12] have used TRNSYS for the dynamic modelling of the SPACS as it allows to model complex algorithms. Redpath et al. [13] reported that using TRNSYS is quite effective in analyzing solar cooling systems for buildings and offices.

Ghaddar et al. [14] presented a a ration of 23.3m^2 of solar collector area per ton of refrigeration with the help of simulation for Beirut. Much research has been conducted to optimize absorption cooling systems through the collector type and optimum storage tank capacity [15], [16]. Pintaldi et al. [17] reviewed TES technologies for solar absorption cooling and control approaches. They highlighted the significant difference in specific storage size when applied in different applications. Raut and Kalamkar [18] reviewed latent TES and concluded that the integration of latent TES extends the operation time of SPACS.

Assilzadeh et al. [19] conducted a study involving the modeling and dynamic simulation of a LiBr-H₂O solar absorption cooling system employing evacuated tube solar collectors under the climatic conditions of Malaysia. Their findings underscored the significance of a 0.8m^3 hot storage tank volume, 35m^2 of evacuated tube solar collectors, and a 20° collector slope for ensuring continuous operation and heightened efficiency in a 3.5kW absorption system. In a different study, Bellos et al. [20] carried out an exhaustive energy and economic analysis of a solar cooling system intended to fulfill the cooling demands of a standard 100m^2 building across diverse climates. The investigation encompassed ten distinct locations, with each location undergoing financial optimization of the system. The outcomes revealed that, among these locations, Abu Dhabi and Phoenix emerged as the most viable choices due to their lower leveled cost of cooling. Altun and Kilic [21] reported an economic feasibility analysis of a single-effect absorption cooling system under environmental conditions in Turkey. They showed a minimum payback period of 10.7 years, whereas the minimum LCOE was 0.128 €/kWh . Al-Ugla et al. [22] reported from their techno-economic analysis that solar thermal cooling is more feasible than solar PV cooling, and feasibility further increases with the scale of operation. They reported a payback period of 18 years for solar thermal cooling compared to 23 years for solar PV cooling. In another study, Sadi et al. [23] reported a payback period of 11 years for SPACS to preserve agricultural products. Behzadi et al. [23] presented a techno-economic analysis of a novel hybrid solar-biomass-fired absorption cooling system and reported an LCOE of $0.047\text{ \$/kWh}$. Hence, for the system, economic feasibility is a lot on the scale of operation for SPACS, whereas integration of a type of TES is essential for consistent operation.

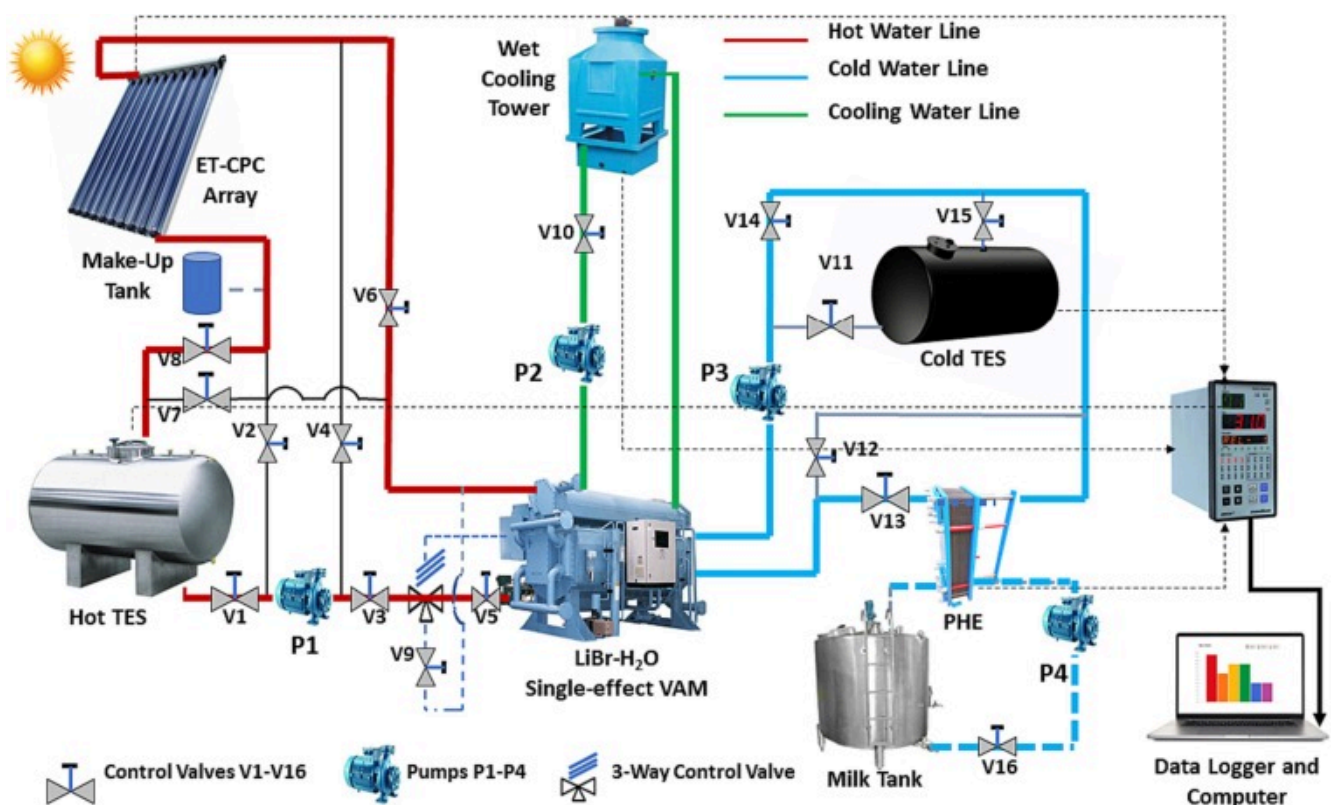
Throughout the cited literature, no studies investigated the solar thermal driven vapor absorption cooling system for milk chilling integrated with sensible thermal energy storage in hot climates.

Therefore, this study investigates the optimization and thermo-economic performance of a solar-powered vapor absorption cooling system integrated with sensible thermal energy storage for milk chilling installed and operated in Jaipur (India) through a dynamic model by using response surface methodology to model a real vapor absorption machine (VAM) incorporated with the experimental

data. The weather data for 2022 is used in performance and productivity analysis. Further, year-round system analysis has been reported for the performance and productivity of individual components and as a whole and the system economic analysis for the system's viability. The novelty of this research lies in estimating the production and productivity of the solar absorption cooling system by dynamic modelling using response surface methodology for actual weather year-round data for Jaipur, India region.

2. System description

The real-size prototype and experimental setup for the solar-powered vapor absorption machine (VAM) are installed on the front lawn of the Mechanical Engineering Department of MNIT, Jaipur, India, having coordinates 26.86N, 75.81 E. As shown in Fig. 1, the setup consists of ET-CPC solar field, VAM, hot TES, cold TES, a plate heat exchanger, and a milk tank. The solar field has a total of 27 ET-CPC modules. Each module is of a 3m² aperture, constituting a total of 81 m² of aperture, which are arranged in seven rows, each having four ET-CPCs in series except one row with three ET-CPCs. This solar field is connected to the hot TES and VAM with the help of a piping system, constituting a solar loop of the whole system. In this setup, a 17.5kW single-effect LiBr-H₂O VAM is installed and driven produced by the collected heat energy from ET-CPC solar field. The VAM rejects the absorption and condensing heat to the environment through a wet cooling tower of 75kW capacity. There are two sensible TES (soft water as a storage medium) integrated with this system; one is hot TES (2.2m³), and another is cold TES (1.1m³). The specifications of various components are detailed in Table 1. The power consumption of various components has been shown in Table 2. The system was installed in 2018 and has been operating flawlessly ever since.



[Download: Download high-res image \(456KB\)](#)

[Download: Download full-size image](#)

Fig. 1. System layout of solar-powered absorption cooling system.

Table 1. Technical description of the various components in the system.

Sr. No.	Description	Unit	Technical Specification
Solar Collectors (ET-CPC) Model: CPC1518			
	No. of evacuated tubes	nos.	18
	η_0 as per EN12975	%	64.2
	Heat transfer coefficient (a_1)	(W/m ² K)	0.89
	Temperature-dependent transfer Coefficient (a_2)	(W/m ² K ²)	0.001
	Grid dimensions	m	2.08×1.64×0.10
	Aperture area	m ²	3.41
	Max Working pressure	bar	10
	Max Stagnation temperature	°C	250
	Glass Tube Material		Borosilicate Glass 3.3
	Selective Absorber coating material		Aluminium Nitride
	Glass Tube ($\Phi_{Ext}/\Phi_{Int}/$ Wall Thickness/Tube length)	mm	47/37/1.6/1500
	Make		Linuo-Ritter
Vapor Absorption Machine (Thermax-5G1AH)			
	Rated Cooling Capacity	kW	17.5
	Dimensions	m	1.67×1.4×1.820
CHW Loop	Inlet Temperature	°C	7
	Outlet Temperature	°C	3.5
	Flow rate	m ³ /hr	4.3
CW Loop	Inlet Temperature	°C	32
	Outlet Temperature	°C	36.2
	Flow rate	m ³ /hr	10
HW Loop	Inlet Temperature	°C	90
	Outlet Temperature	°C	85
	Flow rate	m ³ /hr	5.5

Hot TES Tank

Sr. No.	Description	Unit	Technical Specification
	Diameter	m	1
	Length	m	3.5
	Volume	m ³	2.2
	Material		Mild Steel
	Insulation Material		Fiberglass of 50mm thickness clad with aluminum sheet
	Orientation		Horizontal

Cold TES Tank

Diameter	m	1
Length	m	1.75
Volume	m ³	1.1
Material		Mild Steel
Insulation Material		Nitrile poly-urethane rubber of 25 mm thickness
Orientation		Horizontal

Cooling Tower

Capacity	kW	75
Tower Dimensions	mm	900×900 x 2400
Fan Diameter	mm	550

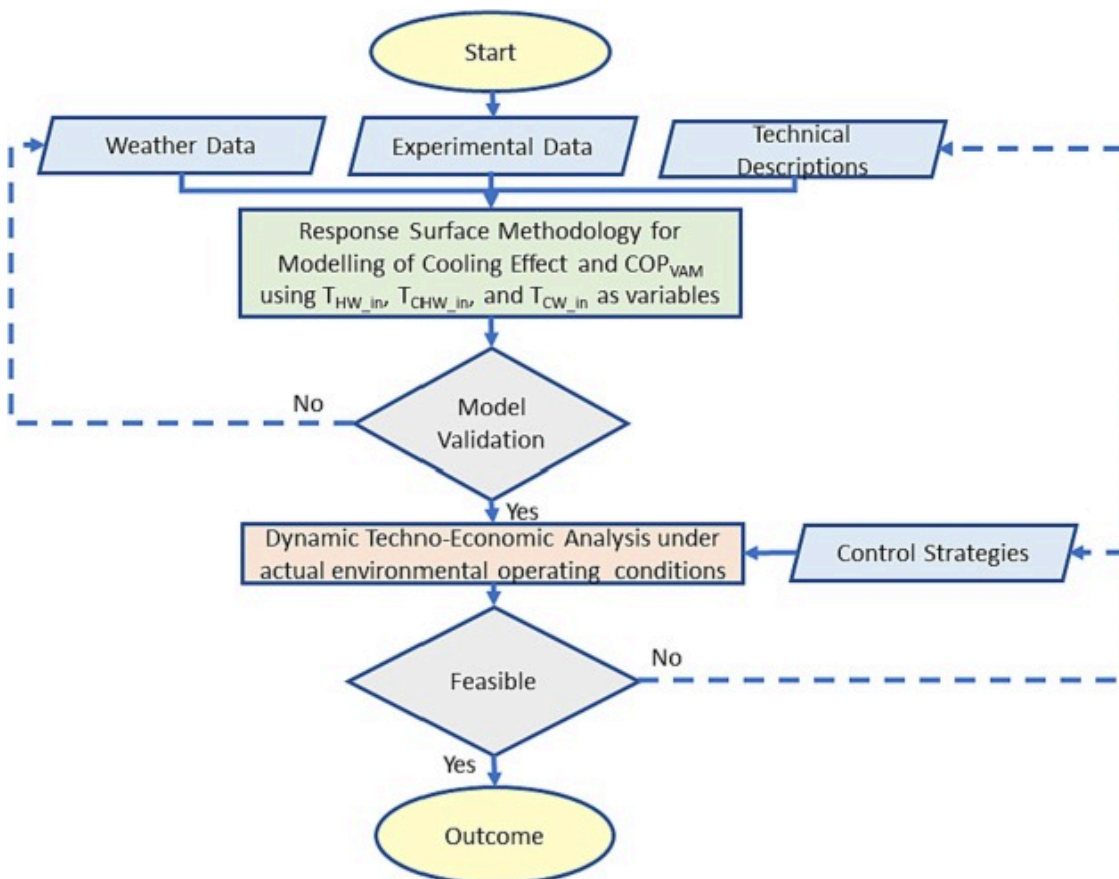
Table 2. Electricity Consumption of the Solar-Powered VAM System.

Sr. No.	Description	Technical Specifications	Power Consumption
1	Vapor Absorption Machine	17.5kW Cooling Capacity	0.4kW
1	Hot Water Pump	Discharge 5.4m ³ /hr, 25m head	0.750kW
2	Cooling Water Pump	Discharge 10.0m ³ /hr, 25m head	0.750kW
3	Chilled Water Pump	Discharge 4.3m ³ /hr, 25m head	0.375kW
4	Cooling Tower	75kW	0.375kW
5	Auxiliaries	–	0.4kW
Total Power Consumption			3.05kW

The uncertainties or errors associated with different measured parameters and computed values fall within standard limits. When determining useful heat gain, the uncertainty is within $\pm 0.59\%$, and for instantaneous energy efficiency, it's within $\pm 1.16\%$. Additionally, the estimated measurement error for temperature stands at $\pm 0.3\%$, while useful heat gain, cooling capacity, COP, and instantaneous energy efficiency have uncertainties of around $\pm 2.5\%$ to $\pm 2.7\%$.

3. Methodology

The useful energy and energetic efficiency of ET-CPC have been estimated using Eqs (1), (2), (3), (4), (5), (6). The detailed analysis, along with validation of the productivity and performance of ET-CPC solar field, has already been presented by authors in [24]. Further, the modelling of VAM is done with the help of RSM using experimental data collected from machine operations under different modes of operation. The model and its terms have been checked for significance using the analysis of variance (ANOVA) and p-value. After that, regression equations for COP and cooling capacity were validated with the help of experimental data. The regression equations are then used along with the modeled equations of various components. A dynamic approach has been used instead of static information flow, as weather conditions are more likely to change every moment. In this research, a time step of 5 min has been used to analyze the weather data and energy measures, refer Fig. 2 for detailed methodology.



[Download: Download high-res image \(288KB\)](#)

[Download: Download full-size image](#)

Fig. 2. Methodology with the flow of information for RSM and techno-economic analysis.

Further, different productivity and performance measures have been estimated on a monthly basis by recognizing typical days, as discussed earlier. The environment of Jaipur, Rajasthan, is primarily hot,

and there are nearly 300 to 330 days of clear sunshine in a year. In this study, 320 days have been recorded as clear sunshine. In the latter section, economic analysis has also been reported using the expected system life, operation, and maintenance, and the cooling effect produced. The levelized cost of energy (LCOE) has been identified as an economic parameter along with a simple and discounted payback period.

4. Analysis of performance and productivity of various components of SPACS

4.1. ET-CPC solar field

a. Useful energy gain

The outlet temperature ($T_{out,n}$) from the n^{th} ET-CPCs coupled in series is estimated as presented in [25]. The values of various parameters have been taken from Table 3.

$$T_{out,n} = \frac{(A_c F_R \alpha \tau)_1}{\dot{m}_f C_f} \times \frac{(1 - K_{eff})^n}{(1 - K_{eff})} I_T + \frac{(A_r F_R U_L)_1}{\dot{m}_f C_f} \times \frac{(1 - K_{eff})^n}{(1 - K_{eff})} T_{amb} + K_{eff}^n T_{in} \quad (1)$$

Where,

$$K_{eff} = 1 - \frac{A_r F_R U_L}{\dot{m}_f C_f} \quad (2)$$

$$F_R = \frac{\dot{m}_f C_f}{U_L A_r} \left[1 - \exp\left(-\frac{2\pi r L U_L}{\dot{m}_f C_f}\right) \right] \quad (3)$$

Table 3. Design parameters of ET-CPC field.

Parameter	Value
R	0.0185m
C_f	4186J/kg.K
L	1500mm
A_r	0.1734m ²
A	0.2215m ²
$A_{c,total}$	81m ²
n	12
τ	0.95
α	0.80
ρ_f	997kg/m ³
\dot{m}_f	0.0357 (kg/s)
U_{tpa}	2.1W/m ² .K
h_{pf}	100W/m ² .K

Parameter	Value
F'	0.986

Useful heat gain for the n-tube connected in series is given as:

$$Q_{useful,n} = (\alpha\tau)_{eff} I_T - (UA)_{eff} (T_{in} - T_{amb}) \quad (4)$$

Where,

$$(\alpha\tau)_{eff} = A_c F_R \alpha\tau \left(\frac{1 - K_{eff}^n}{1 - K_{eff}} \right) \quad (5)$$

$$(UA)_{eff} = A_r F_R U_L \left(\frac{1 - K_{eff}^n}{1 - K_{eff}} \right) \quad (6)$$

b. Instantaneous energetic efficiency

Instantaneous energetic efficiency ($\eta_{Instantaneous}$) is given as

$$\eta_{Instantaneous} = \frac{Q_{useful,n}}{\eta_{opt} \times A_{c,total} \times I_T} \quad (7)$$

4.2. Vapor absorption Machine (VAM)

a. Cooling capacity

The cooling capacity of VAM is calculated using the temperature gradient of chilled water using the following relation:

$$Q_{Cooling} = m_{CHW} * C_{p,CHW} (T_{CHW_{in}} - T_{CHW_{out}}) \quad (8)$$

b. Heat supplied to the generator

The Heat supplied to the generator of VAM is estimated with the help of temperature drop across the hot water line with the help of the given equation:

$$Q_{Generator} = m_{HW} * C_{p,HW} (T_{HW_{in}} - T_{HW_{out}}) \quad (9)$$

c. Thermal coefficient of performance of VAM

The performance of VAM is characterized thermodynamically as the thermal coefficient of performance (COP) of VAM and calculated as per the given relation:

$$COP_{VAM} = \frac{Q_{Cooling}}{Q_{Generator} + E_{Total}} \quad (10)$$

d. Energy efficiency ratio (EER)

The energy efficiency ratio (EER) is an essential performance measure of cooling systems of this nature and is calculated as follows

$$EER = \frac{Q_{Cooling}}{E_{VAM} + E_{Pumps} + E_{Aux} + E_{CT}} \quad (11)$$

Where E_{VAM} , E_{Pumps} , E_{Aux} , and E_{CT} are electricity consumed by VAM, pumps, data loggers, and compressors for hot water control valve openings and cooling towers, respectively.

4.3. Thermal energy storage

The thermal energy storage (TES) performance is shown as charging/discharging efficiency and calculated below [26], [27]. A transient heat transfer model has been used in this study [28].

$$Q_{in, TES} - Q_{loss, TES} = \Delta U_{charging} \quad (12)$$

Where

$$Q_{in, TES} = m_{HW} C_{p, HW} (T_{out, n} - T_{in})$$

$$Q_{loss, TES} = A_{TES} k_{insulation} \frac{(T_{avg, TES} - T_{amb})}{b} \cdot dt$$

$k_{insulation}$, the thermal conductivity of insulation is 0.040W/m-K, and A_{TES} is 11.46m²,

b is the thickness of insulation which is 50mm,

and

$$Q_{useful, n} = m_{TES} C_{p, HW} \frac{dT_{avg, TES}}{dt}$$

a. Charging efficiency

$$\eta_{charging} = \frac{\text{Energy accumulated in TES}}{\text{Energy Input}} = \frac{\Delta U_{charging}}{Q_{in, TES}} \quad (13)$$

b. Discharge efficiency

$$\eta_{discharging} = \frac{\text{Energy recovered by TES}}{\text{Energy released by TES}} = \frac{Q_{rec}}{Q_{rec} + Q_{loss, TES}} \quad (14)$$

4.4. Economic analysis

a. Levelized cost of energy

The levelized cost of energy (LCOE) is the cost of a unit of energy (\$/kWh) produced or saved by the system over its entire useful life, discounted back to the present value. The LCOE for the system has a useful life of N years can be calculated using the relation [29]:

$$LCOE = \frac{TLCC}{E_N} \left[\frac{1 - (1+r)^{-N}}{r} \right] \quad (17)$$

The capital cost of the components of SPACS has been shown in [Table 11](#), whereas the operating cost, as calculated above, comes for the electrical power consumed per year. The system's useful life is 25years, and a discount rate (r) of 6% has been taken [24].

b. Payback period

There are two approaches to calculating payback periods: a simple payback period (SPBP) which takes no account of the discount rate, and a discounted payback period (DPBP). The calculation for both PBPs has shown here:

$$SPBP = \frac{CC}{CF} \quad (18)$$

$$DPBP = \frac{\ln\left(\frac{1}{1 - \frac{CC*r}{CF}}\right)}{\ln(1+r)} \quad (19)$$

5. RSM design for VAM modelling

Response surface methodology (RSM) stands as a extensively employed mathematical and statistical approach for both modeling and dissecting processes wherein the desired outcome is influenced by multiple variables. The primary aim of employing this technique revolves around the optimization of these [30]. In this study, a VAM is modelled to know the effect of hot water (T_{HW_in}), chilled water (T_{CHW_in}), and cooling water (T_{CW_in}) inlet temperatures on the cooling capacity ($Q_{Cooling}$) and COP. Therefore, this study uses a central composite design (CCD) to build a second-order model for response variables. As per the characteristics of the VAM, the range of THW_in is kept between 95 and 70°C whereas TCHW_in ranges between 4 and 24°C and TCW_in ranges from 21 to 32°C. Furthermore, this will improve the performance of the VAM by controlling these variables at an optimum level. As can be seen from Table 4, a total of 20 runs have been managed for this RSM design with three independent variables and two responses, as discussed earlier. These responses have been achieved from many test runs of VAM under various environmental conditions to nullify the impact of extraneous variables.

Table 4. Design of response surface methodology.

Std	Run	A: T_{HW_in}	B: T_{CHW_in}	C: T_{CW_in}	R ₁ : $Q_{Cooling}$	R ₂ : COP_{VAM}
8	1	90	20	32	17	0.5
6	2	90	8	32	10	0.3
13	3	82.5	14	21	17	0.5
15	4	82.5	14	28	14	0.39
17	5	82.5	14	28	15	0.42
9	6	70	14	28	8	0.25
1	7	75	8	24	10	0.28
2	8	90	8	24	14	0.45
3	9	75	20	24	15	0.4
14	10	82.5	14	35	12	0.38
7	11	75	20	32	13	0.33

Std	Run	A: T_{HW_in}	B: T_{CHW_in}	C: T_{CW_in}	R_1 : $Q_{Cooling}$	R_2 : COP_{VAM}
11	12	82.5	4	28	6	0.2
4	13	90	20	24	19	0.55
20	14	82.5	14	28	15	0.43
12	15	82.5	24	28	17	0.5
5	16	75	8	32	8	0.2
16	17	82.5	14	28	14.5	0.41
19	18	82.5	14	28	14	0.38
10	19	95	14	28	18	0.53
18	20	82.5	14	28	15	0.42

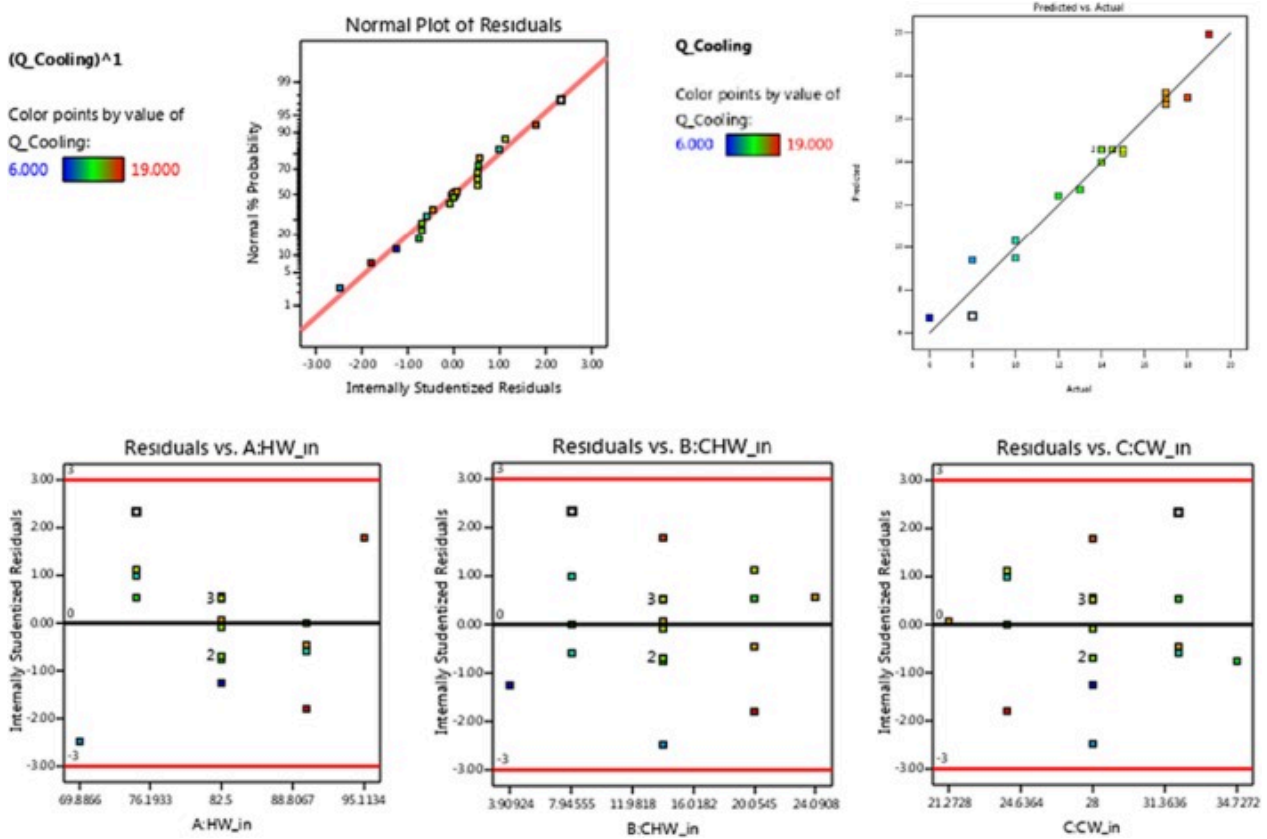
This can be noted that the value of R^2 for the Quadratic model is 0.9664, which shows that data points are very close to the model, refer to Table 5. The alignment between the Predicted R^2 of 0.7720 and the Adjusted R^2 of 0.9361 is notable, given the disparity being below 0.2. Please refer to Table 6 for details. Adequate Precision gauges the signal-to-noise ratio, where a ratio surpassing 4 is preferable. With a signal-to-noise ratio of 20.74, a satisfactory signal is evident. You can find the normal plot of residuals for $Q_{cooling}$ illustrated in Fig. 3.

Table 5. Model selection of Cooling Capacity of VAM.

Source	Sequential p-value	Lack of Fit p-value	Adjusted R^2	Predicted R^2	
Linear	< 0.0001	0.0105	0.8664	0.8161	
2FI	0.8577	0.0063	0.8447	0.7315	
Quadratic	0.0074	0.0391	0.9361	0.7720	Suggested
Cubic	0.0256	0.2639	0.9792	0.6439	Aliased

Table 6. Details of Model opted for cooling capacity of VAM.

Std. Dev.	0.9017	R^2	0.9664
Mean	13.57	Adjusted R^2	0.9361
C.V. %	6.64	Predicted R^2	0.7720
		Adeq Precision	20.7413



[Download: Download high-res image \(266KB\)](#)

[Download: Download full-size image](#)

Fig. 3. Normal plot of residuals for $Q_{cooling}$.

The model F-value of 31.91, as presented in Table 7, signifies the model's significance. The likelihood of such a substantial F-value arising solely from noise is a mere 0.01%. However, P-values below 0.0500 indicate the importance of model terms. In this scenario, model terms A, B, C, and B2 are deemed significant. Conversely, values exceeding 0.1000 suggest insignificance of model terms. If numerous insignificant model terms are present (excluding those necessary for hierarchy), reducing the model might enhance its performance. Conversely, a lack of fit F-value of 5.73 highlights the significance of the lack of fit. The probability of a lack of fit F-value of this magnitude arising from noise is only 3.91%. Fig. 4 shows the effect of variables on $Q_{Cooling}$.

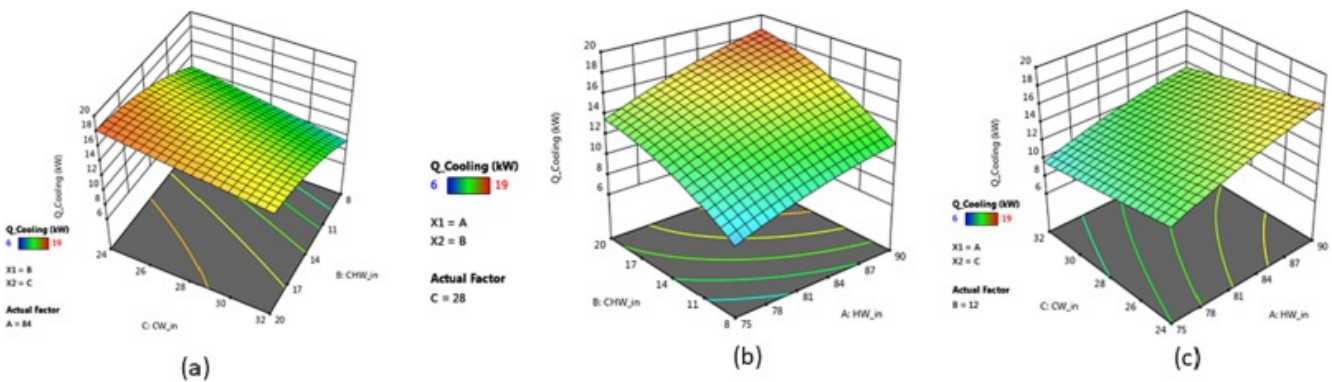
$$Q_{Cooling} \tag{15}$$

$$= [-78.78623 + 1.88429 * T_{HW_in} + 0.535331 * T_{CHW_in} + 0.052212 * T_{CW_in} + 0.005556 * (T_{HW_in} * T_{CHW_in}) - 0.008333 * (T_{HW_in} * T_{CW_in}) + 0.010417 * (T_{CHW_in} * T_{CW_in}) - 0.008654 * (T_{HW_in})^2 - 0.028253 * (T_{CHW_in})^2 + 0.002723 * (T_{CW_in})^2]$$

Table 7. ANOVA for cooling capacity of VAM.

Source	Sum of Squares	df	Mean Square	F-value	p-value	
Model	233.51	9	25.95	31.91	< 0.0001	significant
A- T_{HW_in}	69.54	1	69.54	85.54	< 0.0001	
B- T_{CHW_in}	120.10	1	120.10	147.73	< 0.0001	

Source	Sum of Squares	df	Mean Square	F-value	p-value	
C-T _{CW,in}	24.81	1	24.81	30.52	0.0003	
AB	0.5000	1	0.5000	0.6150	0.4511	
AC	0.5000	1	0.5000	0.6150	0.4511	
BC	0.5000	1	0.5000	0.6150	0.4511	
A ²	3.41	1	3.41	4.20	0.0676	
B ²	14.91	1	14.91	18.34	0.0016	
C ²	0.0273	1	0.0273	0.0336	0.8581	
Residual	8.13	10	0.8130			
Lack of Fit	6.92	5	1.38	5.73	0.0391	significant
Pure Error	1.21	5	0.2417			
Cor Total	241.64	19				



[Download: Download high-res image \(337KB\)](#)

[Download: Download full-size image](#)

Fig. 4. Effect of variables $T_{HW,in}$, $T_{CHW,in}$ and $T_{CW,in}$ on $Q_{Cooling}$.

The value of R^2 for the Quadratic model of the COP for VAM is 0.9725, which shows the closeness of the data points to the model. The Predicted R^2 of 0.8402 shows reasonable concurrence with the Adjusted R^2 of 0.9478, given that the disparity is below 0.2 (Table 8, Table 9). With a signal-to-noise ratio of 23.280, the model displays a satisfactory signal level, surpassing the threshold of 4. Consequently, this model is suitable for guiding exploration within the design space. The normal plot for residuals of COP_{VAM} is shown in Fig. 5.

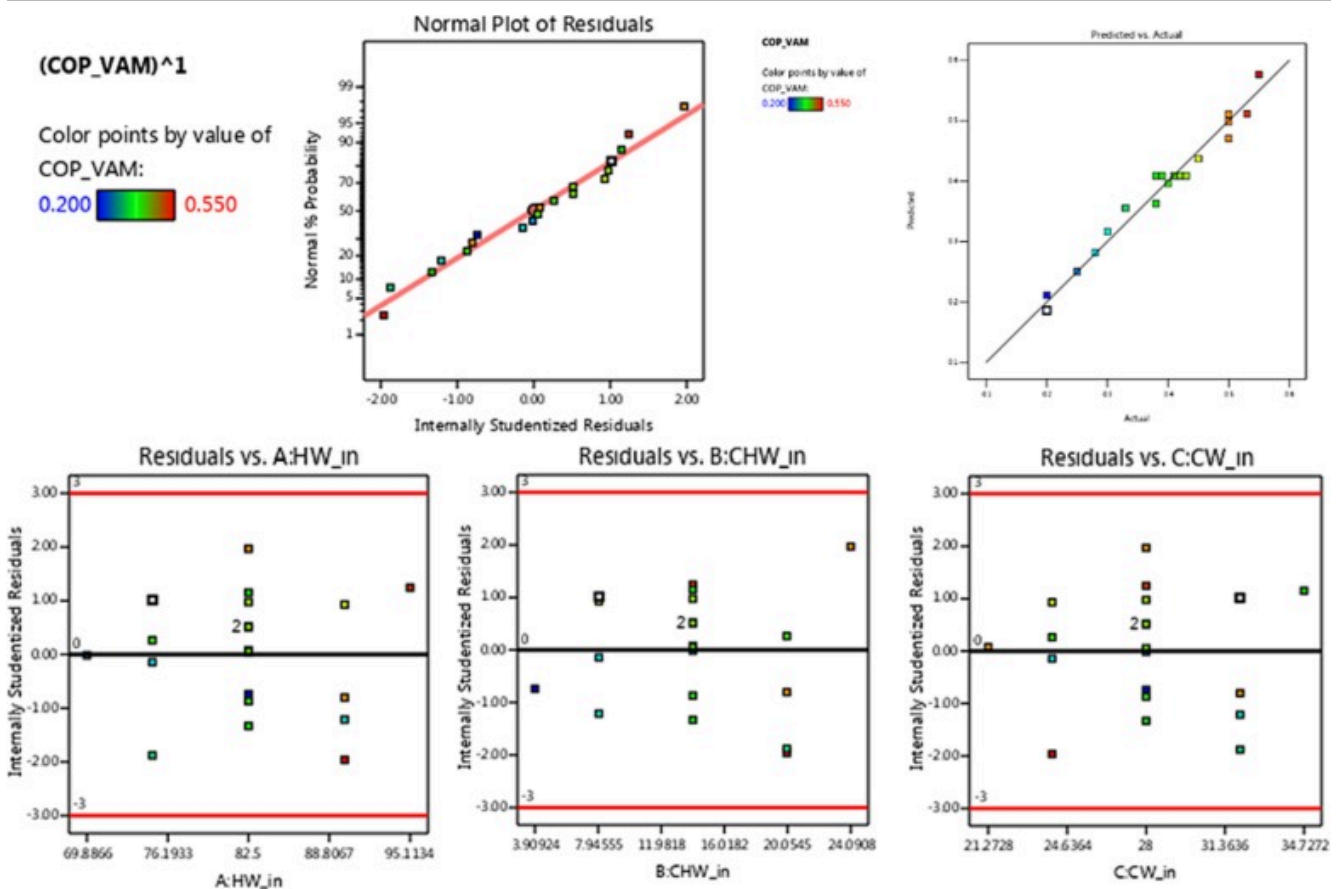
Table 8. Model selection for COP of VAM.

Source	Sequential p-value	Lack of Fit p-value	Adjusted R^2	Predicted R^2
Linear	< 0.0001	0.0674	0.8919	0.8460
2FI	0.6500	0.0493	0.8822	0.7611

Source	Sequential p-value	Lack of Fit p-value	Adjusted R ²	Predicted R ²	
Quadratic	0.0106	0.2342	0.9478	0.8402	Suggested
Cubic	0.2872	0.1966	0.9580	0.0875	Aliased

Table 9. Details of Model selected for COP of VAM.

Std. Dev.	0.0237	R ²	0.9725
Mean	0.3910	Adjusted R ²	0.9478
C.V. %	6.07	Predicted R ²	0.8402
		Adeq Precision	23.2801



[Download: Download high-res image \(309KB\)](#)

[Download: Download full-size image](#)

Fig. 5. Normal plot of residuals for COP of VAM.

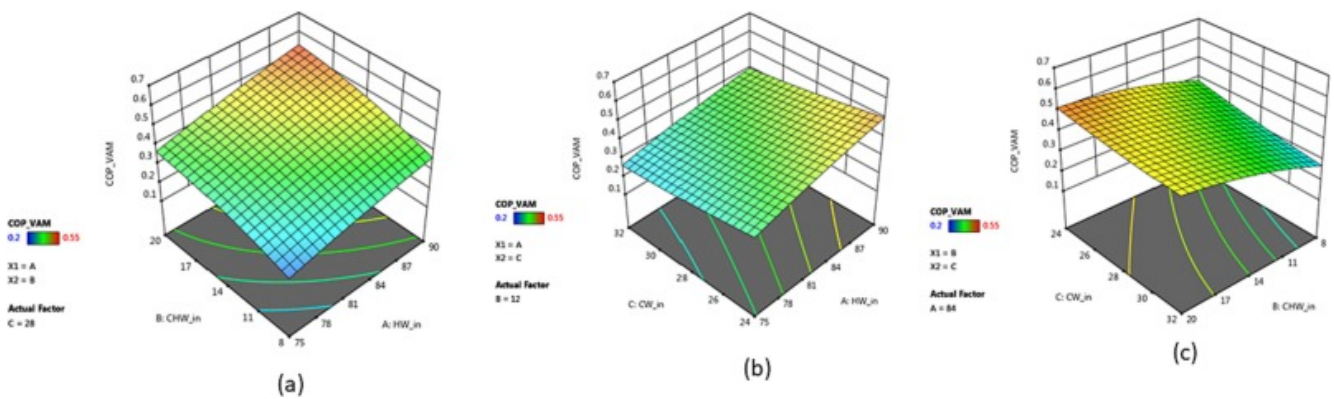
The Model F-value of 39.30 indicates the significance of the model. The probability of encountering such a large F-value purely due to noise is only 0.01% (Table 10). However, model terms are considered significant when their P-values are below 0.0500. In this instance, model terms A, B, C, and B² demonstrate significance. Conversely, values exceeding 0.1000 suggest insignificance for the model terms. With a Lack of Fit F-value of 1.99, the insignificance of the lack of fit is evident compared to the pure error. The occurrence of such a high lack of fit F-value due to noise is

approximately 23.42%. A lack of significant lack of fit is favorable. Fig. 6 shows the effect of variables on output COP_{VAM}.

$$COP_{VAM} = [-1.38601 + 0.043271 * T_{HW_in} + 0.004065 * T_{CHW_in} - 0.028175 * T_{CW_in} + 0.000139 * (T_{HW_in} * T_{CHW_in}) - 0.000208 * (T_{HW_in} * T_{CW_in}) + 0.000573 * (T_{CHW_in} * T_{CW_in}) - 0.000176 * (T_{HW_in})^2 - 0.000668 * (T_{CHW_in})^2 + 0.000486 * (T_{CW_in})^2] \tag{16}$$

Table 10. ANOVA for COP of VAM.

Source	Sum of Squares	df	Mean Square	F-value	p-value	
Model	0.1991	9	0.0221	39.30	< 0.0001	significant
A-HW_in	0.0824	1	0.0824	146.37	< 0.0001	
B-CHW_in	0.0814	1	0.0814	144.62	< 0.0001	
C-CW_in	0.0223	1	0.0223	39.60	< 0.0001	
AB	0.0003	1	0.0003	0.5550	0.4734	
AC	0.0003	1	0.0003	0.5550	0.4734	
BC	0.0015	1	0.0015	2.69	0.1323	
A ²	0.0014	1	0.0014	2.51	0.1445	
B ²	0.0083	1	0.0083	14.79	0.0032	
C ²	0.0009	1	0.0009	1.55	0.2415	
Residual	0.0056	10	0.0006			
Lack of Fit	0.0037	5	0.0007	1.99	0.2342	not significant
Pure Error	0.0019	5	0.0004			
Cor Total	0.2048	19				

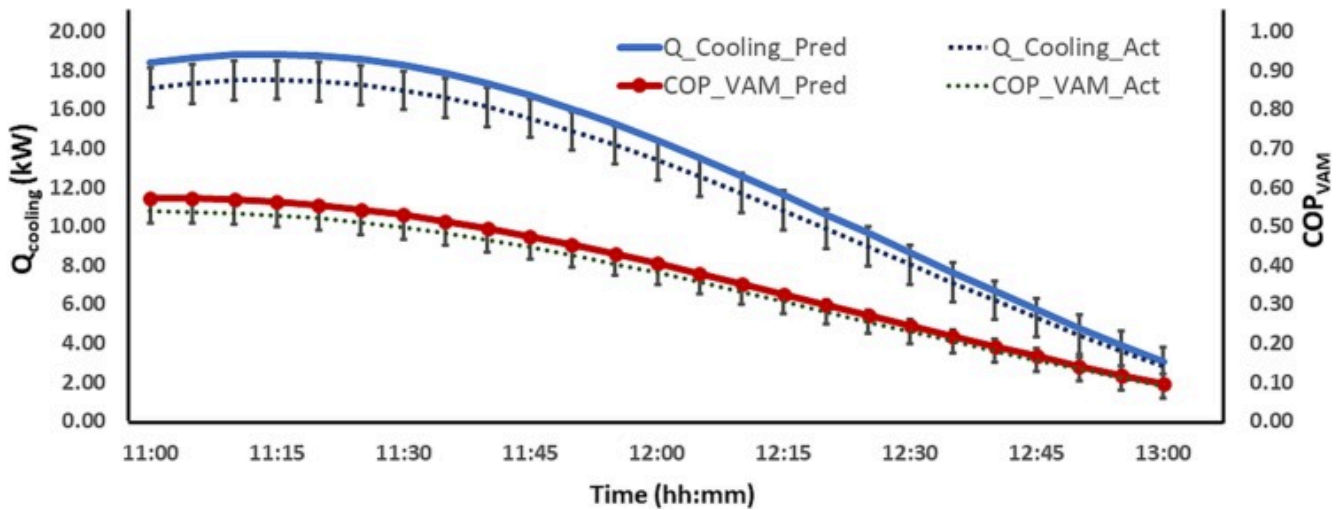


[Download: Download high-res image \(327KB\)](#)

[Download: Download full-size image](#)

Fig. 6. Effect of T_{HW_in}, T_{CHW_in} and T_{CW_in} on COP for VAM.

The model validation is done with the other set of experimental results from VAM, as shown in Fig. 7. It has been noted that the difference between actual and predicted values of cooling capacity and COP_{VAM} are in good agreement as the maximum deviation is 7–8%. Further, the standard error bars have been used to show the standard deviation and margin errors. Thus, the model can be recommended for further estimation of the productivity and performance of SPACS.



Download: [Download high-res image \(211KB\)](#)

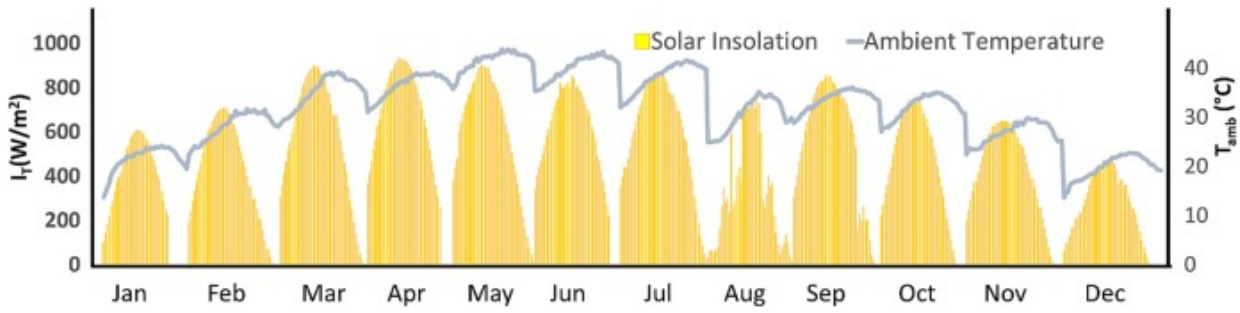
Download: [Download full-size image](#)

Fig. 7. Representation of predicted values through RSM and actual values of cooling capacity and COP.

6. Results and discussions

6.1. Energy analysis of SPACS

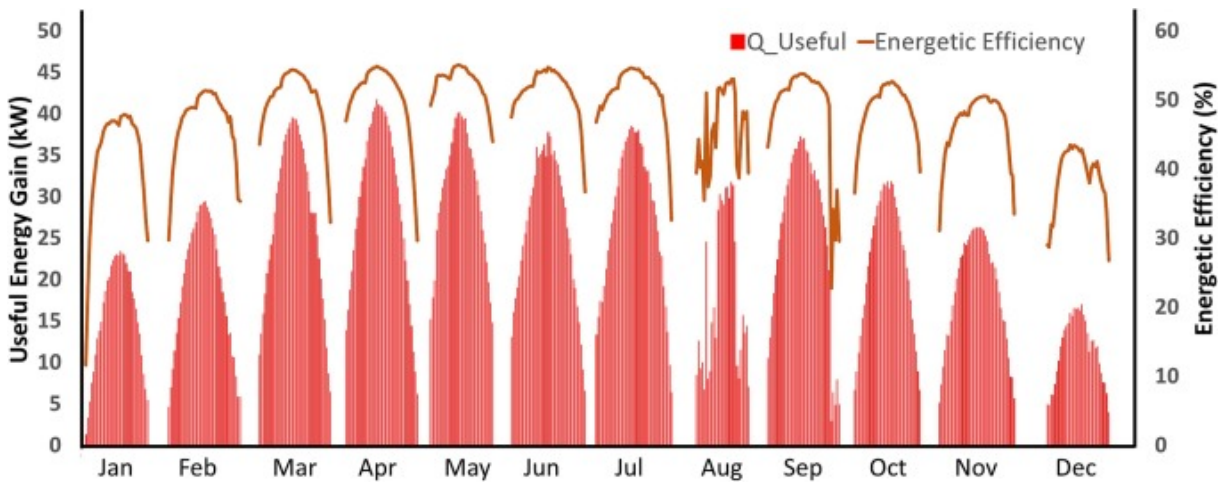
The performance and productivity analysis of solar-powered single-effect vapor absorption cooling systems for milk chilling applications have been reported in this section using RSM. As shown in Fig. 8, solar insolation intensity and ambient temperature are reported for typical days of various months at Jaipur (India) for the year 2022. The typical days are identified, showing the characteristics data of solar insolation, ambient temperature, and relative humidity for a month without undesired disturbances due to any incident. It can be noted from this Figure that winter months from November to February range between 500 and 650W/m² of solar insolation, whereas ambient temperature is below 25°C whereas summer months from March to July have maximum solar insolation up to 900W/m² along with the extended duration of sunshine hours. The monsoon, autumn, and pre-winter months have relatively low solar insolation values; monsoon days are challenging to have sunshine for many weeks. Month-wise analysis has been shown in Fig. 9 for ET-CPC solar field operation reporting useful energy gain and efficiency when operated on a typical operational day of the month. As discussed earlier, the first hot TES is charged from 70°C to 95°C, called system response time (SRT), and shown its values for various months in Fig. 10. The SRT is a direct function of the solar insolation and thermal capacity of TES. Hence, it can be noted that during summer months with the higher solar insolation, SRT has been much less than in monsoon, winter, and pre-winter months. The lowest SRT is recorded in May, whereas up to 1.93 times SRT was reported during winter months.



[Download: Download high-res image \(232KB\)](#)

[Download: Download full-size image](#)

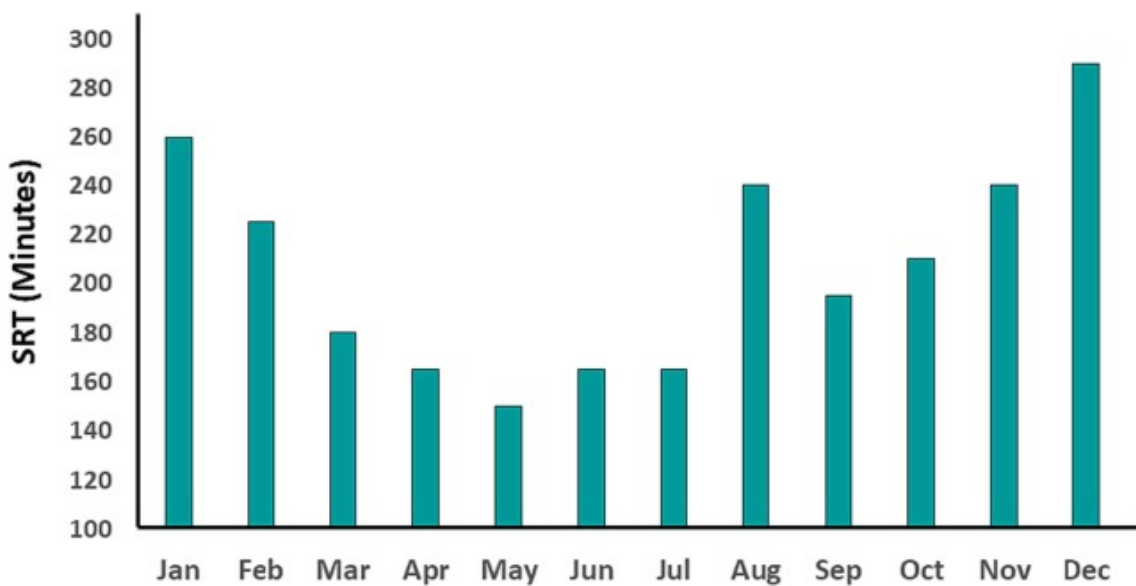
Fig. 8. Month-wise variations of solar insolation and ambient temperature.



[Download: Download high-res image \(437KB\)](#)

[Download: Download full-size image](#)

Fig. 9. Month-wise useful energy gain and energetic efficiency of ET-CPC solar field.

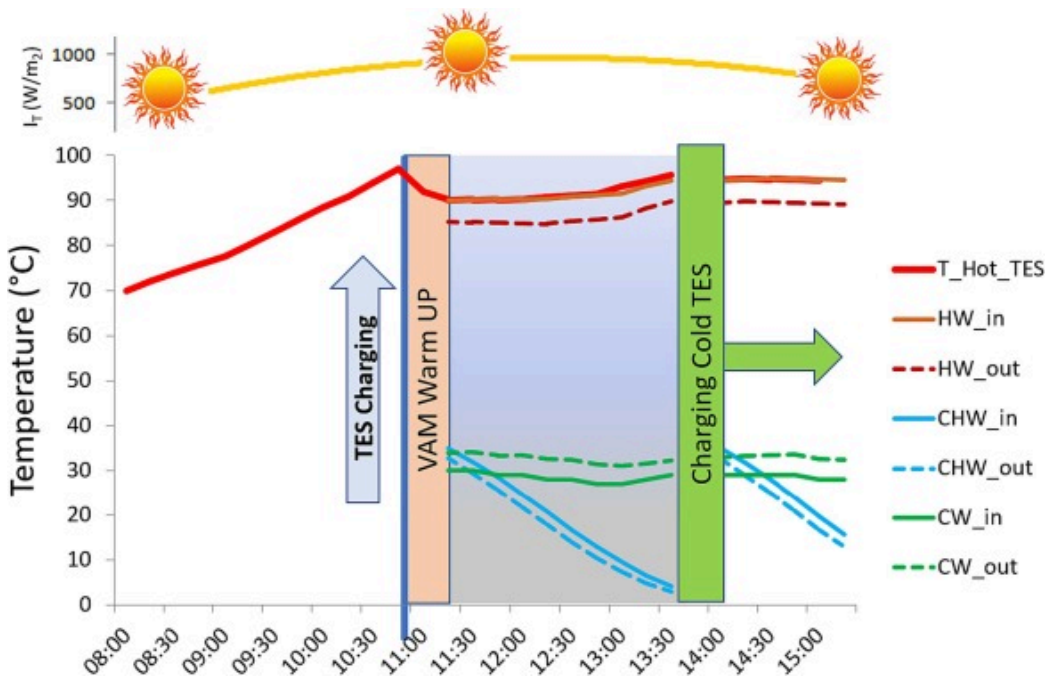


[Download: Download high-res image \(130KB\)](#)

[Download: Download full-size image](#)

Fig. 10. System response time taken to charge hot TES (70 to 95 $^{\circ}C$) during a regular operational day.

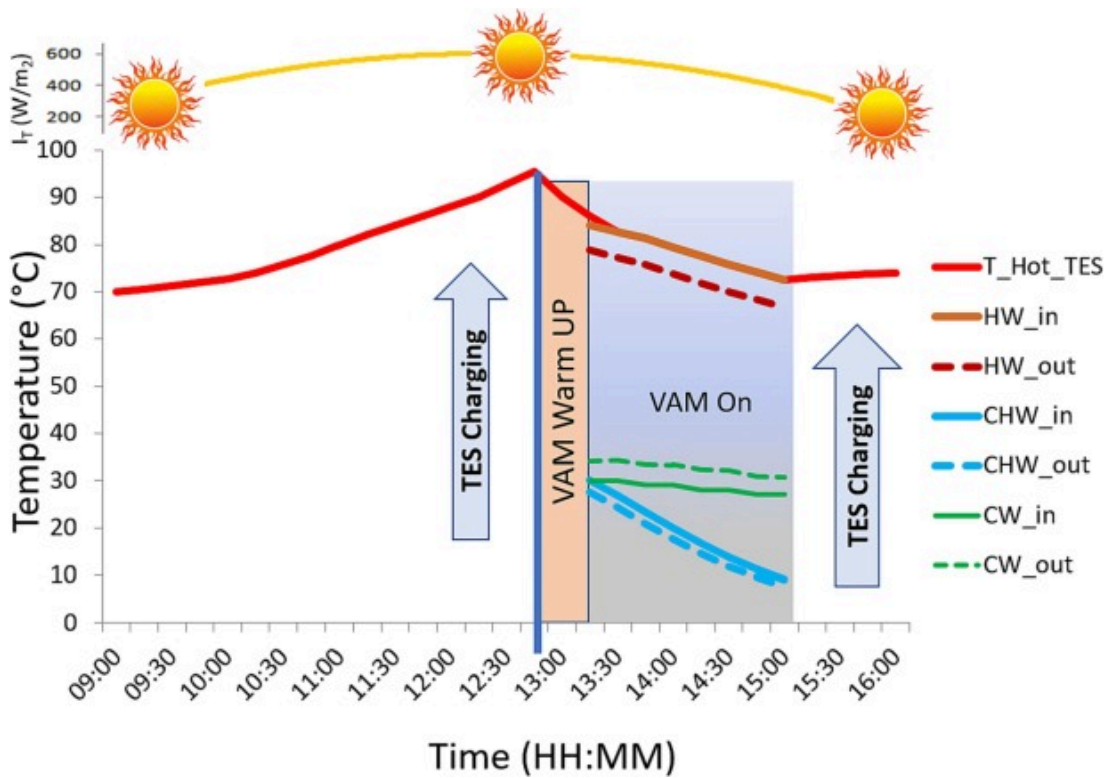
The typical operation of SPACS for summer and winter days are reported in Fig. 11, Fig. 12. It can be reported that there is a sufficient harnessing of solar energy by the ET-CPC solar field, which is quickly charging the TES, and further, VAM has been started and operated for extended working hours. The VAM consumes a significant amount of driving heat energy at the beginning due to its thermal inertia, resulting in a higher temperature drop. Once its generator temperature reaches around 60°C, VAM starts producing a cooling effect unless the hot water supply temperature falls below 70°C or reaches above 95°C. As shown in Fig. 11, summer days are capable of producing desired cooling effect to cool down the 1000l of milk within 3h as per standards ISO 5708 – 2 II, and nevertheless, sufficient heat is still there with the solar loop to charge the 1000l cold storage tank/another milk tank. During winter days, it takes a significant SRT to reach the TES up to 95°C, and after that, VAM operates significantly underperforming due to weak solar insolation; even the SPACS cannot provide first milking, as shown in Fig. 12.



[Download: Download high-res image \(276KB\)](#)

[Download: Download full-size image](#)

Fig. 11. Operation of solar-powered VAM integrated with hot TES during a typical summer day (May 26, 2022).

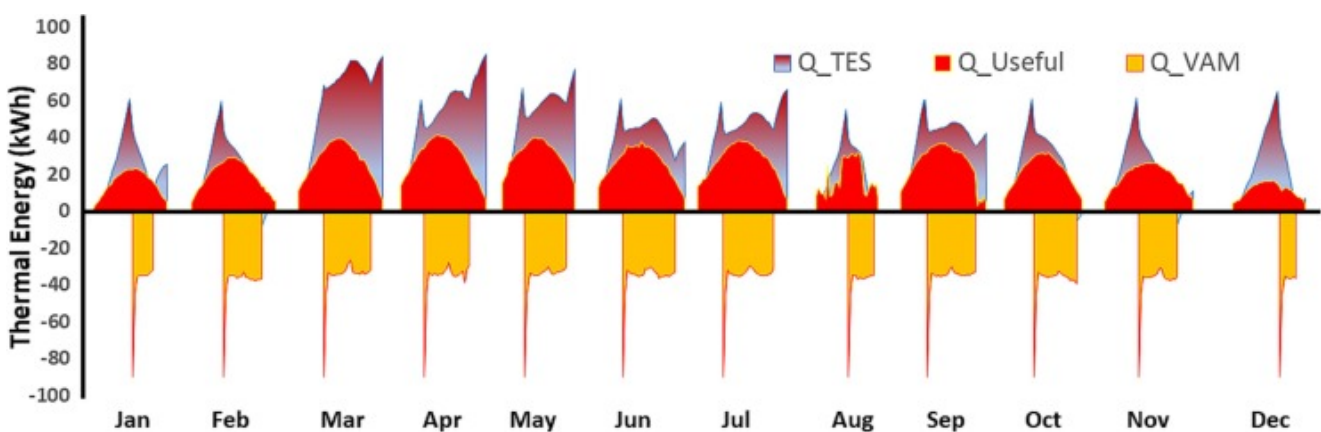


[Download: Download high-res image \(285KB\)](#)

[Download: Download full-size image](#)

Fig. 12. Performance of solar-powered VAM integrated with Hot TES during a typical winter day (Dec 22, 2022).

The role of TES is significantly dominating here to provide thermal balance to meet the demand for VAM generator. The TES has two potential roles here in SPACS; one is as a buffer of energy, and another is to moderate the heat supply between the solar loop and the VAM generator. The TES plays a critical role in reducing the mismatch between supply and demand to improve consistency in performance and productivity. The energy share from/to the TES is reported in Fig. 13.

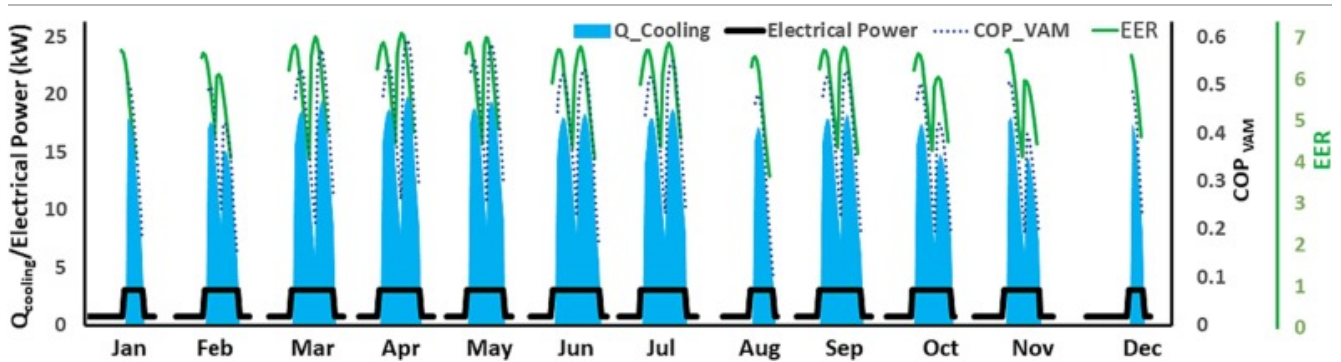


[Download: Download high-res image \(189KB\)](#)

[Download: Download full-size image](#)

Fig. 13. Energy share contribution month-wise between hot thermal energy storage and evacuated tube CPC to operate VAM.

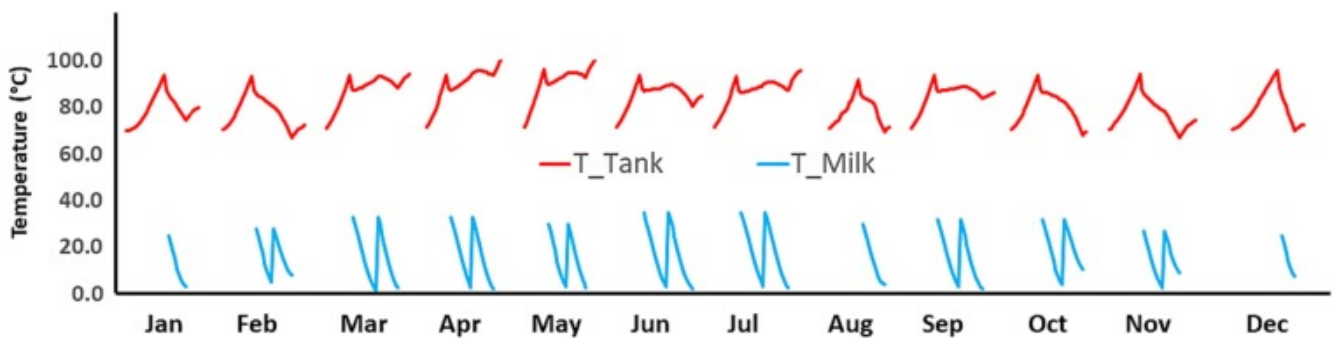
The performance and productivity of VAM are shown here in Fig. 14. Additionally, electrical power consumption is reported to distinguish the operational time for VAM while producing a cooling effect and, at the later stage, estimation of EER. It is clear from the figure that the months Jan, Dec, and Aug cannot provide the required cooling even the first milking of 1000l, whereas the rest of the months are comfortably meeting the first milking cooling requirement and charging the cold TES. The VAM operates satisfactorily to its cooling capacity ranging between 11 and 19kW and the COP ranging maximum up to 0.55. The EER for the VAM operations ranges from 2.5 to 6.5 with an overall average of 4.55 which is far better than the conventional VCR systems. The temperature variations inside the hot TES and milk tank have been reported in Fig. 15, showing significantly better performance for summer months compared to the winter, autumn, and pre-winter months. During summer months, VAM can further be operated even if no sunshine is there as hot TES is charged enough at the end of the day to offer sufficient Heat to the generator of VAM to produce more cooling effect for one more cycle of milk chilling.



[Download: Download high-res image \(244KB\)](#)

[Download: Download full-size image](#)

Fig. 14. Month-wise productivity, performance, and electrical power consumption of solar absorption cooling system for milk chilling application.



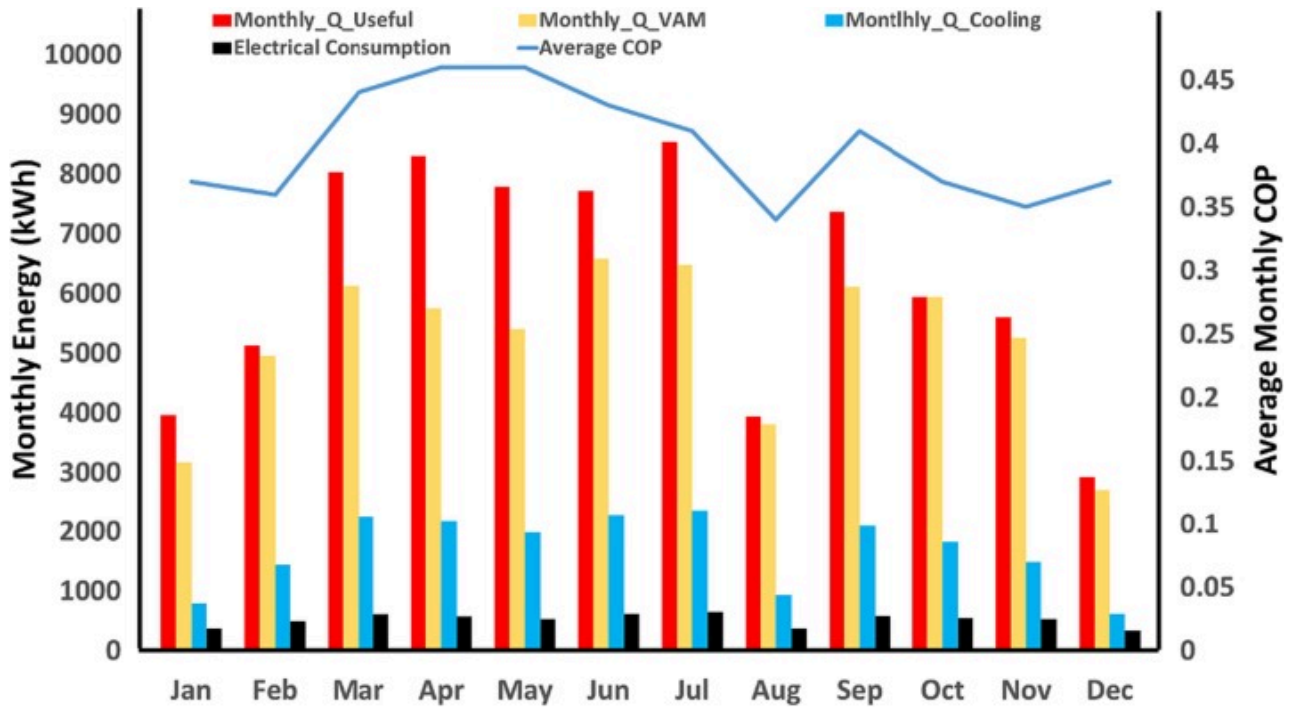
[Download: Download high-res image \(136KB\)](#)

[Download: Download full-size image](#)

Fig. 15. Month-wise variations of the temperature inside hot thermal energy storage and milk chilling.

A comparison of monthly useful energy gain from ET-CPC solar field, Heat utilized by the generator of VAM, produced monthly cooling, and electrical power consumption has been reported in Fig. 16 along with the average monthly COP. It is clear from the comparison that the summer months (March-July) are excellent in both productivity and performance from SPACS. The maximum cooling

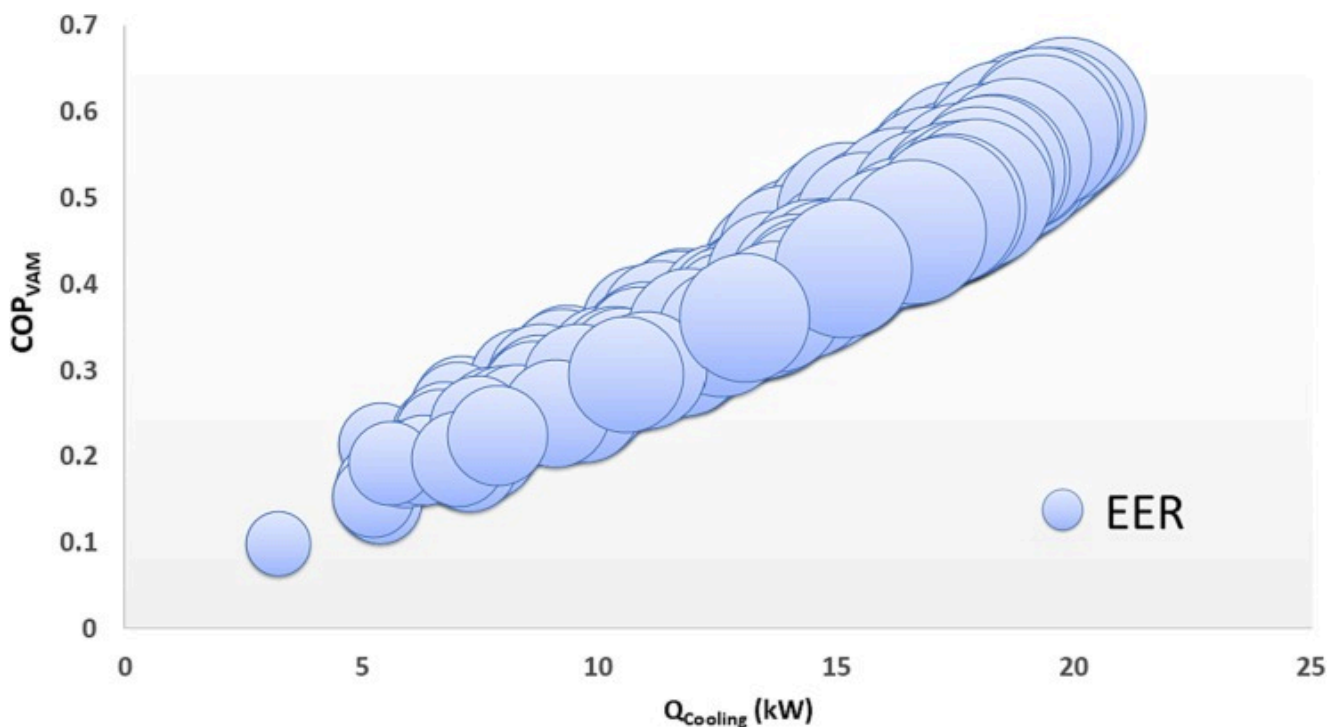
produced is 2356 kWh during July, with an average COP of 0.41. However, April and May report the highest average COP of 0.46. Further, a comparison of EER is shown with the COP and cooling capacity of SPACS in Fig. 17. In this Figure, the bubble's location is shown relative to the COP with a cooling effect, whereas the bubble size shows the value of EER at the point. It is clear from the Figure that bubble accumulation ranges between 11 and 19kW, with COP ranging between 0.3 and 0.55 with an average EER of 4.55.



[Download: Download high-res image \(281KB\)](#)

[Download: Download full-size image](#)

Fig. 16. Monthly energy productivity, performance, and electrical power consumption of solar absorption cooling system.



[Download: Download high-res image \(197KB\)](#)

[Download: Download full-size image](#)

Fig. 17. EER and COP_{VAM} effect with produced cooling effect.

6.2. Economic analysis

The economic analysis encompasses a range of economic metrics, including metrics like SPBP, DPBP, and LCOE. This analysis is conducted using the TLCC, which factors in components like initial capital expenditure, ongoing operational and maintenance costs, interest rates, and projected escalations in electricity prices over time. The SPBP calculated for SPACS is 12.4 years, whereas DPBP is 19.7 years. The results shown in [Table 11](#) indicated that the LCOE for the SPACS has been estimated as 0.177 \$/kWh, whereas the simple payback period is 12.4 years, and the discounted payback period is 19.7 years. The reference case is taken as decentralized milk bulk coolers (with an average COP ranging from 2.7 to 3.0) run by diesel generators, which typically operate with a LCOE of 0.3 to 0.5 \$/kWh [31], [32]. Therefore the cost of milk cooling is taken as 0.19 \$/kWh. Moreover, the involvement of latent TES increases the system's first cost but may help lower the LCOE and PBP further.

Table 11. Capital cost of the system components.

S No	Component	Capacity	Unit	Cost	Remarks
1	Vapor Absorption System	17.5kW	\$	18,692	M/s Thermax Ltd, Pune
2	Solar CPC Collectors	81m ²	\$	10,000	M/s Linuo Ritter Inc.
3	Hot Storage Tank	2.2m ³	\$	1538	M/s Pratap Energy, Jaipur
4	Cold Storage Tank	1.1m ³	\$	1184	M/s Pratap Energy, Jaipur
5	Milk Heat Exchanger	25 plates	\$	538	M/s Kelvion, Pune
6	Pumps	4 nos.	\$	384	M/s Kirloskar, Pune
7	Cooling Tower	70kW	\$	350	M/s Sumangal, Jaipur
8	Interconnecting Piping & Valves		\$	1538	M/s Gupta Pipe, Jaipur
9	Milk Storage Tank	1m ³	\$	1754	M/s Star Engg., Meerut
Total			\$	35,978	

7. Conclusions and future scope of work

The dynamic modelling of a solar-powered single-effect LiBr-H₂O system integrated with sensible thermal energy storage is reported in this study, in which VAM is modelled using RSM with the help of experimental data. Further, a year-round month-wise analysis of productivity and performance of SPACS for milk chilling applications has been reported along with economic analysis. Following conclusions are drawn from this study.

- a. The model F-value of 31.91 and 39.30 for cooling capacity and COP_{VAM} , respectively, shows that RSM modelling is significant with an appropriate value of R^2 .
- b. The performance of individual components, such as ET-CPC solar field, VAM, etc., have been investigated, and it was found that individual components are working as per the specifications as ET-CPC energetic efficiency is recorded with a maximum value of 54%. In contrast, the COP of VAM is recorded as 0.55.
- c. The operation of SPACS in summer months is relatively consistent and performed with high productivity and performance with maximum values of 2356 kWh and 0.55 monthly, respectively, whereas a maximum average monthly COP is recorded as 0.46.
- d. The operation of SPACS during pre-winter and monsoon months is inconsistent and underperforming due to significant variations in weather conditions and low solar insolation. The cooling produced during these months is as low as 620 kWh monthly, whereas the maximum average COP recorded is 0.34.
- e. The EER for the SPACS operations ranges from 2.5 to 6.5 with an overall average of 4.55 which is far better than the conventional VCR systems.
- f. The LCOE for the SPACS has been estimated as 0.177 \$/kWh, whereas the simple payback period is 12.4years, and the discounted payback period is 19.7years.

The integration of SPACS with latent TES may be further helpful to increase the operational time of VAM and reduce the SRT of TES, which may result in better thermal management. However, the involvement of latent TES contributes to increasing the system's first cost but may be useful in further lowering the LCOE and PBP. The control strategies are very impactful while operating SPACS; therefore, optimum control strategies must be studied to improve productivity and performance.

Ethical approval

We confirm that this work has not been published elsewhere, nor is it currently under consideration for publication elsewhere.

Consent to participate

Authors give their consent to participate.

Consent to publish

We consent to publish in the Environmental Science and Pollution Research after acceptance.

Funding

There are no funding disclosures to make.

Availability of data and materials

Calculations data and other relevant material would be made available to the editor/reviewer as and when required.

CRedit authorship contribution statement

Dinesh Kumar Sharma: Conceptualization, Data curation, Formal analysis, Investigation, Methodology, Validation, Visualization, Writing – original draft. **Dilip Sharma:** Project administration, Resources, Software, Supervision, Writing – review & editing. **Ahmed Hamza H. Ali:** Project administration, Resources, Supervision, Writing – review & editing.

Declaration of Competing Interest



The authors declare that they have no known competing financial interests or personal relationships that could have appeared to influence the work reported in this paper.

[Recommended articles](#)

Data availability

Data will be made available on request.

References

- [1] R. Narayanan, G.K. Harilal, S. Golder
Feasibility study on the solar absorption cooling system for a residential complex in the Australian subtropical region
Case Stud Therm Eng (2021), p. 27, [10.1016/j.csite.2021.101202](https://doi.org/10.1016/j.csite.2021.101202) ↗
[View in Scopus](#) ↗ [Google Scholar](#) ↗
- [2] A. Alahmer, S. Ajib
Solar cooling technologies: state of art and perspectives
Energy Convers Manag (2020), p. 214, [10.1016/j.enconman.2020.112896](https://doi.org/10.1016/j.enconman.2020.112896) ↗
[Google Scholar](#) ↗
- [3] N.I. Ibrahim, F.A. Al-Sulaiman, F.N. Ani
Solar absorption systems with integrated absorption energy storage—a review
Renew Sustain Energy Rev, 82 (2018), pp. 1602-1610, [10.1016/j.rser.2017.07.005](https://doi.org/10.1016/j.rser.2017.07.005) ↗
 [View PDF](#) [View article](#) [View in Scopus](#) ↗ [Google Scholar](#) ↗
- [4] N.I. Ibrahim, M.M.A. Khan, I.M. Mahbulul, R. Saidur, F.A. Al-Sulaiman
Experimental testing of the performance of a solar absorption cooling system assisted with ice-storage for an office space
Energy Convers Manag, 148 (2017), pp. 1399-1408, [10.1016/j.enconman.2017.07.001](https://doi.org/10.1016/j.enconman.2017.07.001) ↗
 [View PDF](#) [View article](#) [View in Scopus](#) ↗ [Google Scholar](#) ↗
- [5] O. Ayadi, S. Al-Dahidi

Comparison of solar thermal and solar electric space heating and cooling systems for buildings in different climatic regions

Sol Energy, 188 (2019), pp. 545-560, [10.1016/j.solener.2019.06.033](https://doi.org/10.1016/j.solener.2019.06.033) ↗

 [View PDF](#) [View article](#) [View in Scopus](#) ↗ [Google Scholar](#) ↗

- [6] Kohlenbach P, Dennis M, Director I. Solar cooling in Australia: the future of air-conditioning? *Ecolibrium Aust Inst Refrig Air Cond Heat (Formerly AIRAH Journal)* 2010.

[Google Scholar](#) ↗

- [7] M. Beccali, M. Cellura, P. Finocchiaro, F. Guarino, S. Longo, B. Nocke
Life cycle assessment performance comparison of small solar thermal cooling systems with conventional plants assisted with photovoltaics

Energy Procedia, 30 (2012), pp. 893-903, [10.1016/j.egypro.2012.11.101](https://doi.org/10.1016/j.egypro.2012.11.101) ↗

 [View PDF](#) [View article](#) [View in Scopus](#) ↗ [Google Scholar](#) ↗

- [8] V. Mittal, K.S. Kasana, N.S. Thakur
Modelling and simulation of a solar absorption cooling system for India

J Energy South Africa (2006), p. 17, [10.17159/2413-3051/2006/v17i3a3290](https://doi.org/10.17159/2413-3051/2006/v17i3a3290) ↗

[Google Scholar](#) ↗

- [9] F. Assilzadeh, S.A. Kalogirou, Y. Ali, K. Sopian
Simulation and optimization of a LiBr solar absorption cooling system with evacuated tube collectors

Renew Energy, 30 (8) (2005), pp. 1143-1159, [10.1016/j.renene.2004.09.017](https://doi.org/10.1016/j.renene.2004.09.017) ↗

 [View PDF](#) [View article](#) [View in Scopus](#) ↗ [Google Scholar](#) ↗

- [10] M.S.A. Khan, A.W. Badar, T. Talha, M.W. Khan, F.S. Butt
Configuration based modeling and performance analysis of single effect solar absorption cooling system in TRNSYS

Energy Convers Manag, 157 (2018), pp. 351-363, [10.1016/j.enconman.2017.12.024](https://doi.org/10.1016/j.enconman.2017.12.024) ↗

 [View PDF](#) [View article](#) [View in Scopus](#) ↗ [Google Scholar](#) ↗

- [11] Z.Y. Xu, R.Z. Wang
Simulation of solar cooling system based on variable effect LiBr-water absorption chiller. *Renew*

Energy, 113 (2017), pp. 907-914, [10.1016/j.renene.2017.06.069](https://doi.org/10.1016/j.renene.2017.06.069) ↗

 [View PDF](#) [View article](#) [View in Scopus](#) ↗ [Google Scholar](#) ↗

- [12] M. Asim, J. Dewsbury, S. Kanan
TRNSYS simulation of a solar cooling system for the hot climate of Pakistan







Energy Procedia, 91 (2016), pp. 702-706, [10.1016/j.egypro.2016.06.233](https://doi.org/10.1016/j.egypro.2016.06.233) ↗

 [View PDF](#) [View article](#) [View in Scopus](#) ↗ [Google Scholar](#) ↗

- [13] D. Redpath, A. Paneri, H. Singh, A. Ghitas, M. Sabry
Design of a building-scale space solar cooling system using TRNSYS

Sustain (2022), p. 14, [10.3390/su141811549](https://doi.org/10.3390/su141811549) ↗

[Google Scholar](#) ↗

- [14] N.K. Ghaddar, M. Shihab, F. Bdeir
Modeling and simulation of solar absorption system performance in Beirut
Renew Energy, 10 (1997), pp. 539-558, [10.1016/S0960-1481\(96\)00039-0](https://doi.org/10.1016/S0960-1481(96)00039-0) ↗
 [View PDF](#) [View article](#) [View in Scopus](#) ↗ [Google Scholar](#) ↗
- [15] C. Sanjuan, S. Soutullo, M.R. Heras
Optimization of a solar cooling system with interior energy storage
Sol Energy, 84 (7) (2010), pp. 1244-1254, [10.1016/j.solener.2010.04.001](https://doi.org/10.1016/j.solener.2010.04.001) ↗
 [View PDF](#) [View article](#) [View in Scopus](#) ↗ [Google Scholar](#) ↗
- [16] R. Hirmiz, M.F. Lightstone, J.S. Cotton
Performance enhancement of solar absorption cooling systems using thermal energy storage with phase change materials
Appl Energy, 223 (2018), pp. 11-29, [10.1016/j.apenergy.2018.04.029](https://doi.org/10.1016/j.apenergy.2018.04.029) ↗
 [View PDF](#) [View article](#) [View in Scopus](#) ↗ [Google Scholar](#) ↗
- [17] S. Pintaldi, C. Perfumo, S. Sethuvenkatraman, S. White, G. Rosengarten
A review of thermal energy storage technologies and control approaches for solar cooling
Renew Sustain Energy Rev, 41 (2015), pp. 975-995, [10.1016/j.rser.2014.08.062](https://doi.org/10.1016/j.rser.2014.08.062) ↗
 [View PDF](#) [View article](#) [View in Scopus](#) ↗ [Google Scholar](#) ↗
- [18] D. Raut, V.R. Kalamkar
A review on latent heat energy storage for solar thermal water-lithium bromide vapor absorption refrigeration system
J Energy Storage (2022), p. 55, [10.1016/j.est.2022.105828](https://doi.org/10.1016/j.est.2022.105828) ↗
[Google Scholar](#) ↗
- [19] F. Assilzadeh, S.A. Kalogirou, Y. Ali, K. Sopian
Simulation and optimization of a LiBr solar absorption cooling system with evacuated tube collectors
Renew Energy, 30 (2005), pp. 1141-1159, [10.1016/j.renene.2004.09.017](https://doi.org/10.1016/j.renene.2004.09.017) ↗
[Google Scholar](#) ↗
- [20] E. Bellos, C. Tzivanidis
Energetic and financial analysis of solar cooling systems with single effect absorption chiller in various climates
Appl Therm Eng, 126 (2017), pp. 809-821, [10.1016/j.applthermaleng.2017.08.005](https://doi.org/10.1016/j.applthermaleng.2017.08.005) ↗
 [View PDF](#) [View article](#) [View in Scopus](#) ↗ [Google Scholar](#) ↗
- [21] A.F. Altun, M. Kilic
Economic feasibility analysis with the parametric dynamic simulation of a single effect solar absorption cooling system for various climatic regions in Turkey
Renew Energy, 152 (2020), pp. 75-93, [10.1016/j.renene.2020.01.055](https://doi.org/10.1016/j.renene.2020.01.055) ↗
 [View PDF](#) [View article](#) [View in Scopus](#) ↗ [Google Scholar](#) ↗
- [22] A.A. Al-Ugla, M.A.I. El-Shaarawi, S.A.M. Said, A.M. Al-Qutub

Techno-economic analysis of solar-assisted air-conditioning systems for commercial buildings in Saudi Arabia

Renew Sustain Energy Rev, 54 (2016), pp. 1301-1310, [10.1016/j.rser.2015.10.047](https://doi.org/10.1016/j.rser.2015.10.047) ↗

 [View PDF](#) [View article](#) [View in Scopus](#) ↗ [Google Scholar](#) ↗

[23] A. Behzadi, A. Arabkoohsar, M. Sadi, K.H. Chakravarty

A novel hybrid solar-biomass design for green off-grid cold production, techno-economic analysis and optimization

Sol Energy, 218 (2021), pp. 639-651, [10.1016/j.solener.2021.02.065](https://doi.org/10.1016/j.solener.2021.02.065) ↗

 [View PDF](#) [View article](#) [View in Scopus](#) ↗ [Google Scholar](#) ↗

[24] D.K. Sharma, D. Sharma, A.H.H. Ali

Energy, exergy, environmental impact, and economic analyses of evacuated tube compound parabolic concentrator-powered solar thermal domestic water heating system

Environ Sci Pollut Res, 29 (54) (2022), pp. 82390-82410, [10.1007/s11356-022-21505-2](https://doi.org/10.1007/s11356-022-21505-2) ↗

[View in Scopus](#) ↗ [Google Scholar](#) ↗

[25] R.K. Mishra, V. Garg, G.N. Tiwari

Thermal modeling and development of characteristic equations of evacuated tubular collector (ETC)

Sol Energy, 116 (2015), pp. 165-176, [10.1016/j.solener.2015.04.003](https://doi.org/10.1016/j.solener.2015.04.003) ↗

 [View PDF](#) [View article](#) [View in Scopus](#) ↗ [Google Scholar](#) ↗

[26] M.A. Rosen, I. Dincer

Exergoeconomic analysis of power plants operating on various fuels

Appl Therm Eng, 23 (2003), pp. 643-658, [10.1016/S1359-4311\(02\)00244-2](https://doi.org/10.1016/S1359-4311(02)00244-2) ↗

 [View PDF](#) [View article](#) [View in Scopus](#) ↗ [Google Scholar](#) ↗

[27] Dincer I, Rosen MA. Exergy: energy, environment and sustainable development; 2007. [10.1017/CBO9781107415324.004](https://doi.org/10.1017/CBO9781107415324.004).

[Google Scholar](#) ↗

[28] Dinesh Kumar Sharma, D. Sharma, A.H.H. Ali

Exergy destructions analysis of evacuated tube compound parabolic concentrator

Appl Sol Energy (English Transl Geliotekhnika), 57 (5) (2021), pp. 420-429, [10.3103/S0003701X2105011X](https://doi.org/10.3103/S0003701X2105011X) ↗

[View in Scopus](#) ↗ [Google Scholar](#) ↗

[29] L. Miller, R. Carriveau, S. Harper, S. Singh

Evaluating the link between LCOE and PPA elements and structure for wind energy

Energy Strateg Rev, 16 (2017), pp. 33-42, [10.1016/j.esr.2017.02.006](https://doi.org/10.1016/j.esr.2017.02.006) ↗

 [View PDF](#) [View article](#) [View in Scopus](#) ↗ [Google Scholar](#) ↗

[30] M.K. Kamarulzaman, A. Abdullah

Multi-objective optimization of diesel engine performances and exhaust emissions characteristics of *Hermetia illucens* larvae oil-diesel fuel blends using response surface methodology

Energy Sources, Part A Recover Util Environ Eff (2020), [10.1080/15567036.2020.1849450](https://doi.org/10.1080/15567036.2020.1849450) ↗

[Google Scholar](#) ↗

- [31] M. Solano-Peralta, M. Moner-Girona, W.G.J.H.M. van Sark, X. Vallvè
“Tropicalisation” of Feed-in Tariffs: a custom-made support scheme for hybrid
PV/diesel systems in isolated regions

Renew Sustain Energy Rev, 13 (9) (2009), pp. 2279-2294, [10.1016/j.rser.2009.06.022](https://doi.org/10.1016/j.rser.2009.06.022) ↗

 [View PDF](#) [View article](#) [View in Scopus](#) ↗ [Google Scholar](#) ↗

- [32] S.N. Sapali, S.M. Pise, A.T. Pise, D.V. Ghewade
Investigations of waste heat recovery from bulk milk cooler

Case Stud Therm Eng, 4 (2014), pp. 136-143, [10.1016/j.csite.2014.09.003](https://doi.org/10.1016/j.csite.2014.09.003) ↗

 [View PDF](#) [View article](#) [View in Scopus](#) ↗ [Google Scholar](#) ↗

Cited by (7)

[Grooved single-channel dual media tank thermal energy storage systems to improve overall thermal performance: Numerical analysis](#)

2025, Alexandria Engineering Journal

[Show abstract](#) ✓

[Recent developments in solar-powered refrigeration systems and energy storage methods for on-farm preservation of fruits and vegetables](#)

2024, Sustainable Energy Technologies and Assessments

[Show abstract](#) ✓

[Blade height impact on self-starting torque for Darrieus vertical axis wind turbines](#)

2024, Energy Conversion and Management: X

[Show abstract](#) ✓

[Advancing energy transition with novel biomass-solar based multigeneration energy system using hydrogen and storage options for sustainable cities](#)

2024, Sustainable Cities and Society

Citation Excerpt :

...Combined with their high efficiency achieved through isentropic compression and expansion processes that minimize energy loss, engineers are continually working on the development of Brayton thermodynamic cycle systems. Absorption cooling systems are efficient methods for cooling applications (Sharma et al., 2023). These systems come in various types....

[Show abstract](#) ✓

[Experimental Study on Performance of a Solar Thermal- Driven Vapor Absorption System Integrated With Hot Thermal Energy Storage for Milk Chilling](#) ↗

2024, Journal of Solar Energy Engineering, Transactions of the ASME

Fostering solar hybrid cooling systems in MENA region: A techno-economic and emission reduction assessment ↗

2024, AIP Advances



[View all citing articles on Scopus ↗](#)

© 2023 The Authors. Published by Elsevier Ltd.



All content on this site: Copyright © 2024 Elsevier B.V., its licensors, and contributors. All rights are reserved, including those for text and data mining, AI training, and similar technologies. For all open access content, the Creative Commons licensing terms apply.

